Battery Operation Informed Temperature Prediction for Cooling-Aware Microgrid Day-Ahead Scheduling

David Okpo
Student Member, IEEE
McNeese State University
Lake Charles,
LA, USA
dokpo@mcneese.edu

Jose Betancourt
Member, IEEE
McNeese State University
Lake Charles,
LA, USA
msu-jbetancour1@mcneese.edu

Cunzhi Zhao
Member, IEEE
McNeese State University
Lake Charles,
LA, USA
czhao@mcneese.edu

***Abstract*— High renewable penetration in microgrids increases variability and operational uncertainty, making Battery Energy Storage Systems (BESS) central to balancing supply and demand, providing reserves, and improving reliability. Traditional day-ahead schedules (TDAS) typically model BESS as an electrical-only resource with fixed efficiency, power limits, and state-of-charge (SoC) bounds, overlooking battery thermal dynamics and the electricity required for cooling. This omission can steer the dispatch toward options that look cheap on paper but hide the real costs of thermal management. In this paper, a cooling-aware aware day-ahead scheduling (CDAS) framework that embeds a data-driven BESS temperature predictor and associated cooling-power model into the economic dispatch is proposed. First, a deep neural network (DNN) trained on real operational data forecasts BESS temperature is developed. Second, predicted temperatures parameterize a cooling-power calculation that is integrated into the DAS, ensuring the plan internalizes the electrical cost of thermal management while respecting equipment and reliability constraints. Furthermore, this paper compares the resulting schedule against a conventional electrical-only baseline to assess impacts on projected cost, feasibility, and operating profiles. The approach provides a practical pathway for aligning microgrid planning with the physical realities of BESS operation, improving dispatch realism without sacrificing tractability.**

Index Terms—Battery Energy Storage Systems, Battery Temperature, Day-Ahead Scheduling, Deep Neural Network, HVAC, Microgrids.

NOMENCLATURE

Sets

S_K	Set of Time intervals.

Parameters

c_G	Generation cost of a generation source.
C^{MG}	Total operating cost of the microgrid over the scheduling horizon.
c_{NL}^{G}	No load cost for the generation source.
c_{SU}^{G}	Start-up cost for the generation source.
ΔK	Change in time.
R_{prcnt}	Percentage of the backup power to the total power.
E_{Max}^{S}	Maximum energy capacity of ESS.
E_{Min}^{S}	Minimum energy capacity of ESS.
ΔT	Change in temperature.
c_k^{Buy}	Wholesale purchase price in time interval k.
c_k^{Sell}	Wholesale sell price in time interval k.
P_{Max}^{G}	Maximum capacity of generator.
P_{Min}^{G}	Minimum capacity of generator.
P_{Max}^{Grid}	Maximum thermal limit of tie-line between main grid and microgrid in kW.
E_{Max}^{Grid}	Maximum thermal limit of tie-line between main grid and microgrid in kWh.
P_{Ramp}^{G}	Ramping limit of diesel generator.
P_{Max}^{S}	Maximum charge/discharge power of BESS.
P_{Min}^{S}	Minimum charge/discharge power of BESS.
η_{Disc}^{S}	Discharge efficiency of BESS.
η_{Char}^{S}	Charge efficiency of BESS.
P_{HVAC}	Power rating of the HVAC.
$\dot{Q}_{max}^{hvac}$	Maximum cooling heat rate in kW.
m_{bat}	Mass of battery in kg.
c_p^{bat}	Specific heat capacity of battery.
COP	Coefficient of performance.
T_{spt}	Desired temperature.

Variables

U_k^{Buy}	Status of buying energy in time interval k.
U_k^{Sell}	Status of selling energy in time t.
U_k^{Char}	Charging status of BESS in time interval k.
U_k^{Disc}	Discharging status of BESS in time interval k.
U_k^{G}	Status of generator in time interval k.
V_k^{G}	Startup status indicator in time interval k.
E_k^{G}	Energy generated by generator in time interval t.
P_k^{G}	Power output of generator at time step k
ΔT_{DAS}	Change in temperature in DAS algorithm.
E_k^{hvac}	Energy needed from the HVAC to cool the BESS
ΔK	Length of a single dispatch interval.
E_k^{Buy}	Energy purchased during time interval k in kWh
P_k^{Buy}	Power purchased at time step k in kW.
E_k^{Sell}	Energy sold during time interval k in kWh.
P_k^{Sell}	Power sold to grid at time step k in kW.
U_k^{L}	Load demand during time interval k in kWh
P_k^{L}	Load demand in the microgrid at time step k in kW
ΔK_{hvac}	Time in hours needed for the HVAC to cool the battery to the desired temperature.
Q_{bat}	Thermal energy in kwh to be removed in order to get the battery to the desired temperature.
E_k^{Disc}	Discharging of energy storage system at time k.
E_k^{Char}	Charging of energy storage system at time k.
T_k	Temperature at a particular k.
T_k^{pred}	Predicted temperature from DNN for a period k.

979-8-3315-8138-1

I. Introduction

Microgrids have progressed from experimental pilots to essential infrastructure for campuses, industry, and remote communities [1-3]. They provide two primary benefits: greater reliability and resilience during grid disturbances [4] and improved integration of distributed energy resources such as solar and wind [5]. With decarbonization goals tightening and energy prices growing more volatile, pairing microgrids with renewable generation is now even more routine which while reduces our reliance on fossil powered generators and in turn reduces greenhouse gas emission introduces a new problem in terms of reliability as their output are very variable and uncertain [6]. To combat this, most modern microgrids include a BESS.

A Battery Energy Storage System is an integrated asset that stores electrical energy in batteries and returns it as alternating current through a bidirectional power conversion system [7], coordinated by controls and protection to help it operate safely within its equipment limits. In practice, a BESS shifts energy across hours to align supply with demand, responds quickly to contingencies and ramping needs, and provides reserves and ride through that other assets cannot [7]. In order to co-ordinate these capabilities though, operators develop a DAS [8] that translates forecasts of weather, solar output, ambient temperature, load, and market prices into an hour by hour optimized economic plan. The schedule sets charge and discharge targets, defines a state of charge trajectory, and allocates headroom for reserves. It respects equipment limits, efficiency and loss assumptions, and reliability requirements, while balancing battery actions with onsite generation, grid imports and exports, and any necessary curtailment [9]. As conditions evolve, this schedule anchors real time adjustments so the microgrid can meet cost and reliability objectives with a unified plan that keeps all resources working in stride.

Consequently, the quality of the day ahead schedule largely determines system outcomes, since it regulates how intensively and how often energy is drawn from each resource, with particular relevance for the Battery Energy Storage System. Therefore, creating a DAS algorithm that factors every important physical characteristic of components of the system is of the upmost importance. In practice, however, many existing day ahead scheduling approaches model the assets as purely electrical elements. Batteries in particular are often represented only by round trip efficiency, charge and discharge power limits, and simple state of charge bounds. Schedules derived from this electrical only view can look cheaper on paper because they omit costs and constraints that emerge from real operation. A critical missing element is temperature. During charging and discharging, battery cells generate heat [10], cell resistance changes with temperature, and both efficiency and permissible operating ranges are temperature dependent. To keep the battery within a healthy range and to preserve calendar and cycle life, a dedicated cooling system is required. Whether this is an integrated thermal management unit packaged with the battery racks or a room level ventilation and air conditioning system, it draws additional electrical energy, increases the net load seen by the microgrid, and therefore affects cost [11]. To develop the most optimal DAS, this has to be added to the algorithm.

As expected, a substantial amount of research has been conducted on DAS for systems incorporating a BESS. Liu et al. [12] propose a probabilistic, chance-constrained scheduling model that uses scenario-based MILP to handle renewable and load uncertainty in a grid-connected microgrid with PV, wind, conventional units, and BESS, demonstrating improved robustness of the resulting schedule. More closely related to this work, Shen et al. [14] develop a structured day-ahead microgrid scheduling model that explicitly includes BESS based on both lithium-ion and lead-acid technologies. Their battery model captures degradation rates across different SOC ranges and enforces temperature-related operational constraints, and the resulting mixed-integer linear formulation demonstrates how degradation limits and high summer temperatures can restrict battery dispatch.

Building on this important contribution, this paper shifts the emphasis from temperature only as a constraint on battery operation to temperature as a driver of cooling power consumption and cost that must also be scheduled.

However, incorporating this into the DAS requires a way to predict temperature under the various operating conditions that the battery will experience. Temperature needs to be predicted when the system is charging, discharging, or resting, and when ambient conditions change. These predictions must be available at each time step in the planning horizon so the scheduler can use them consistently. With a clear forecast of temperature at each operating point, the algorithm can check thermal limits, anticipate cooling needs, and assign the appropriate cost or constraints where necessary. This paper addresses that gap by training a deep neural network (DNN) on real BESS operating data to predict temperature under anticipated dispatch conditions. The DNN predictions are then coupled with the improved DAS formulation and compared against a conventional DAS that ignores thermal effects. In summary, this paper aims to contribute the following:

- It develops a DNN-based temperature prediction model and a CDAS formulation that uses these predictions to compute HVAC cooling energy and embed the resulting cooling demand and cost into the microgrid optimization.
- It compares the proposed CDAS against a conventional DAS that neglects cooling costs, showing that ignoring cooling leads to underestimated operating costs and different BESS dispatch patterns.

The remainder of this paper is organized as follows. Section II presents the traditional day-ahead scheduling (TDAS) formulation. Section III introduces the cooling-aware DAS (CDAS) algorithm and its integration with the DNN-based temperature model. Section IV details a case study and the corresponding results. Section V concludes the paper.

II. Traditional DAS Algorithm

In the TDAS, the microgrid is scheduled using a purely electrical day-ahead formulation characterized by constraints (1)–(15). The nodal energy-balance equation (1) enforces that, at every interval, total supply from dispatchable generators, wind, solar, BESS discharge, and grid purchases exactly

979-8-3315-8138-1

matches total demand from loads, BESS charging, and any exports to the main grid, while the objective function in (2) minimizes total operating cost, including generator production, no-load and start-up costs, and net grid energy purchases. Generator operating constraints (3)–(5) restrict each dispatchable unit to remain within its minimum/maximum output limits and respect ramp-rate limits between successive time steps, ensuring physically feasible trajectories. Grid-exchange logic in (6)–(8) prevents simultaneous buying and selling, and caps import and export power by the tie-line rating through binary indicators on the buy/sell decisions. BESS operating-mode constraints (9)–(11) enforce mutually exclusive charging and discharging at each interval and bound charge/discharge power within the rated range of each storage unit. The internal energy evolution of each BESS is governed by (12)–(13), which define the state of charge as a normalized energy variable and update stored energy across time using charge/discharge power and efficiencies, with (14) imposing a terminal condition that the final energy equals the initial level. Finally, the spinning-reserve requirement in (15) guarantees that the combination of unused generator capacity and available grid capacity provides sufficient headroom to cover a specified fraction of the current load, ensuring reliability against contingencies.

Under this TDAS, the optimized schedule for generators, grid exchange, and BESS is obtained without explicitly accounting for the cooling energy required by the BESS. After the fact, an additional HVAC cooling cost is computed for the intervals in which the BESS is used and added to the operating cost as a post-processing step, rather than influencing the dispatch decisions themselves. This omission is explicitly addressed in the proposed CDAS, where the cooling load is embedded directly into the scheduling formulation.

$$E^{Buy}_k + E^G_k + E^{WT}_k + E^{PV}_k + E^{Disc}_k = E^{Sell}_k + E^L_k + E^{Char}_k, \forall k \tag{1}$$

$$C^{MG} = \sum\sum (E^G_k c_G + U^G_k c^G_{NL} + V^G_k c^G_{SU}) + E^{Buy}_k c^{Buy}_k - E^{Sell}_k c^{Sell}_k, \forall k \tag{2}$$

$$P^G_{Min} \leq P^G_k \leq P^k_{Max} \; where \; E = P \cdot \Delta k, \qquad \forall k \tag{3}$$

$$P^G_{k+1} - P^G_k \leq \Delta k \cdot P^G_k, \forall k \tag{4}$$

$$P^G_k - P^G_{k-1} \leq \Delta k \cdot P^G_{Ramp}, \forall k \tag{5}$$

$$U^{Buy}_k + U^{Sell}_k \leq 1, \forall k \tag{6}$$

$$0 \leq P^{Buy}_k \leq U^{Buy}_k \cdot P^{Grid}_{Max}, \forall k \tag{7}$$

$$0 \leq P^{Sell}_k \leq U^{Sell}_k \cdot P^{Grid}_{Max}, \forall k \tag{8}$$

$$U^{Disc}_k + U^{Char}_k \leq 1, \forall k \tag{9}$$

$$U^{Char}_k \cdot P^S_{Min} \leq P^{Char}_k \leq U^{Char}_k \cdot P^S_{Max}, \forall k \tag{10}$$

$$U^{Disc}_k \cdot P^S_{Min} \leq P^{Disc}_k \leq U^{Disc}_k \cdot P^S_k, \forall k \tag{11}$$

$$SOC^S_k = \frac{E^S_k}{E^S_k}, \forall k \tag{12}$$

$$E^S_k - E^S_{k-1} + \Delta K \cdot \left(\frac{P^{Disc}_{k-1}}{\mu^{Disc}_S} - P^{Char}_k \mu^{Char}_S \right) = 0, \forall k \tag{13}$$

$$E^S_{k=24} = E^k_{Initial} \tag{14}$$

$$P^{Grid}_{Max} - P^{Buy}_k + P^{Sell}_k + P^G_{Max} - P^G_k \geq R_{percent} P^L_k \cdot P^k_L \forall k \tag{15}$$

III. Cooling-Aware DAS Algorithm

To incorporate the cooling load, the power-balance constraint in (1) is replaced by the energy-balance formulation in (16), and (17) – (21) are added to compute the HVAC as shown in Fig. 1 cooling energy in each interval.

$$E^{Buy}_k + E^G_k + E^{WT}_k + E^{PV}_k + E^{Disc}_k = E^{Sell}_k + E^L_k + E^{Char}_k + E^{hvac}_k, \forall k \tag{16}$$

The additional term E^{HVAC}_k represents the electrical energy consumed by the HVAC to cool the battery during interval k and is obtained as

$$E^{hvac}_k = P_{hvac} \cdot \Delta K_{hvac} \tag{17}$$

The required cooling duration ΔK_{HVAC} follows from the ratio between the thermal energy that must be removed and the maximum cooling capacity of the HVAC:

$$\Delta K_{HVAC} = \frac{Q_{bat}}{\dot{Q}^{hvac}_{max}} \tag{18}$$

The thermal energy extracted from the battery is modeled as

$$Q_{bat} = m_{bat} \cdot c^{bat}_p \cdot (T^{pred}_k - T_{spt}) \tag{19}$$

where T^{pred}_k is the predicted temperature from the DNN for a period k, T_{spt} is the desired temperature. The maximum cooling capacity of the HVAC($\dot{Q}^{hvac}_{max}$) is related to its electrical rating and coefficient of performance by

$$\dot{Q}^{hvac}_{max} = P_{hvac} \cdot COP \tag{20}$$

The predicted battery temperature used in (19) is produced by the trained neural network model as

$$T^{pred}_k = DNN(E_{mean} \, T_{amb} \, T_{initial}) \tag{21}$$

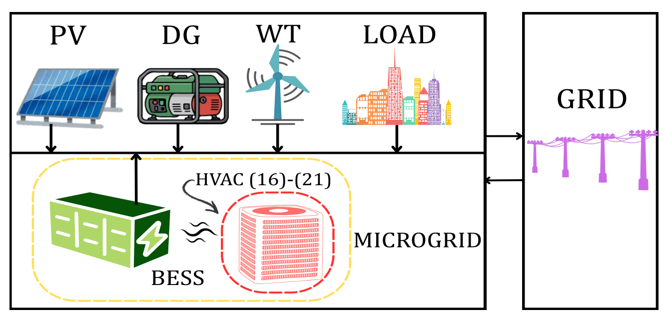

Figure 1. Microgrid case.

IV. Case Study

The microgrid used for this case study consists of solar panels, generators, wind farms, BESS and bidirectional connection to the grid. It can import up to 1,500 kW from the main grid in each hour, with time-varying purchase prices over the 24 hour horizon, and can export surplus energy back to the grid at 0.8 times the corresponding buying price. Three dispatchable generators are available. In addition, the system includes a solar PV plant and a wind generation unit, both modeled via 24-hour availability profiles, and a BESS with a power rating of 300 kW. The associated cooling demand is explicitly represented using an HVAC unit with rated power P_{HVAC} = 30kW and coefficient of performance COP=3.52, cooling a battery pack with mass m_{bat}=24,460kg and specific

979-8-3315-8138-1

heat c_p^{bat} =1.005kJ/kg°C The battery temperature is regulated around a set-point T_{spt} is 24°C, with initial temperature T_1 is 24°C. These parameter values are representative of typical utility-scale BESS installations and commercial HVAC systems. Figure 2 illustrates the 24-hour profiles of system load, aggregate renewable generation, and the resulting net load.

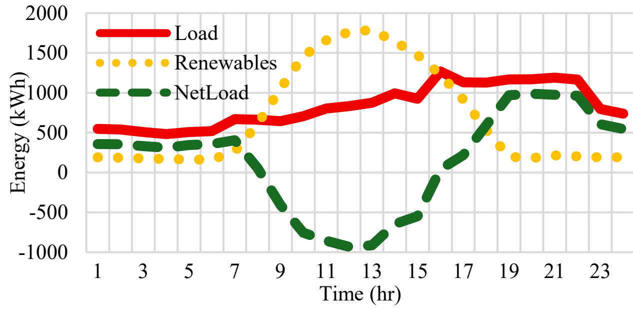

Figure 2. Load Profile.

A. *Training Data of Temperature Prediction*

The DNN is trained on lithium-ion cell data from the NASA Battery Data Library [15], using only charge and discharge profiles with measured voltage, current, temperature, and time. Preprocessing was conducted in two stages beginning with the discharge profile. A MATLAB script extracts discharge cycles, normalizes time, splits them into ~1-hour segments and computes segment-level features duration in hours (D_{Hour}), mean voltage (V_{Mean}), mean current (I_{Mean}), first (T_{first}) and final cell temperature(T_{final}) and ambient temperature (T_{amb}) which are stored in a master table. A Python script then filters out low-quality segments, computes temperature change ($\Delta T_{Data} = T_{final} - T_{first}$) and mean energy ($E_{mean}$) for each segment. This alongside the initial temperature (T_{first}) and ambient temperature (T_{amb}) will serve as input to the deep neural network model while the final cell temperature (T_{final}) serves as the output. The same procedure is applied to charging cycles.

B. *Deep Neural Network*

A DNN is used as a nonlinear regressor to predict the final cell temperature (T_{final}) from aggregated features, capturing the nonlinear dependence on electrical loading and thermal conditions without an explicit thermal model. The model is a compact fully connected multilayer perceptron that maps (E_{mean}, T_{amb}, $T_{initial}$) to the final temperature. Inputs are standardized using the training-set mean and standard deviation. The standardized vector passes through two hidden layers of 16 neurons with ReLU activation, followed by a single linear output neuron that returns the normalized prediction of (T_{final}). In this paper this prediction is referred to as T_k^{pred}.The trained DNN is then linearized (BigM method) and embedded into the microgrid optimization model to predict BESS temperature as a function of scheduled charge and discharge energy. The model achieves an MAE of 2.38 °C.

C. *Results*

The minimum operating cost obtained with the TDAS is \$426.98. Under this baseline schedule, the BESS is discharged during hours 6, 19, 21, and 24 and charged during hours 15, 16, and 22. These charge/discharge events increase battery temperature and would, in practice, trigger additional HVAC cooling energy. To assess robustness against renewable variability, the same 24-hour load profile is evaluated under three levels of renewable availability, obtained by uniformly decreasing the solar and wind profiles to 75%, and 50% of their nominal values. Table 1 shows that in all three renewable-penetration cases the proposed CDAS consistently reduces HVAC energy relative to TDAS. For the 100% renewable base case, CDAS lowers HVAC energy from 82.6 kWh to 60.0 kWh (about 27% reduction) and reduces the total operating cost from \$426.98 to \$423.61 (≈0.8% savings). At 75% renewable penetration, CDAS again cuts HVAC energy (70.2 kWh to 55.5 kWh) while yielding a small but consistent cost reduction relative to TDAS. At 50% penetration, the HVAC energy savings remain on the order of 20%, and the total operating cost under CDAS is essentially unchanged (within 0.1%) compared to TDAS, showing that enforcing the temperature constraint does not materially penalize economic performance even when the system relies more on conventional generation.

Table 1. Sensitivity test with different renewable penetration

Renewable Penetration	E_HVAC (kWh)		Cost (\$)	
	TDAS	CDAS	TDAS	CDAS
100%	82.64	60.01	426.98	423.61
75%	70.17	55.46	1,029.84	1,029.36
50%	69.76	55.46	1,751.41	1,752.47

The following results and analysis are based on the 100% renewable penetration model, which serves as the reference case for Fig. 3–Fig. 5. CDAS co-optimizes the BESS schedule and HVAC operation so that the battery temperature constraint is enforced directly in the dispatch solution rather than checked post compute. Figure 3 compares the predicted battery temperature trajectories under the traditional and cooling-aware schedules for the base case. Under the TDAS, the ex-post thermal evaluation shows that the pack temperature gradually drifts upward and reaches a peak of approximately 40.3 °C by the end of the 24-hour horizon. When the same load and renewable conditions are dispatched using the proposed CDAS, the maximum temperature is 30.7 °C, keeping the battery roughly 10 °C cooler while maintaining the same initial temperature and setpoint. The peak overshoot is significantly mitigated, which is precisely the regime that accelerates degradation and reduces safety margins in utility-scale BESS installations.

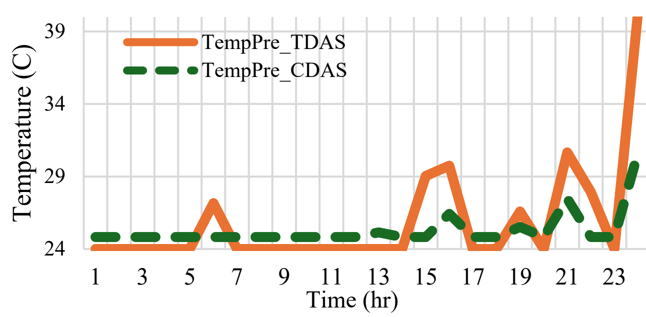

Figure 3. Temperature Prediction Comparison between TDAS and CDAS.

Instead of simply following the most profitable arbitrage opportunities, the CDAS anticipates the additional cooling energy required to remove the heat generated by charging and discharging. As a result, the optimized schedule avoids clustering large charging/discharging events in periods when the HVAC would need to work hardest, and it slightly reduces total BESS output in the base case.

The impact of the cooling-aware formulation on the hourly operating pattern is illustrated in Figures 4 and 5 for the 100% renewable penetration case. Figure 4 shows the scheduled BESS energy output in each hour under the TDAS and the CDAS. Under TDAS, the battery is largely idle for most of the day and then experiences several large, concentrated charge and discharge events, most notably a deep charging period around hours 15–16 followed by large discharges in hours 19, 21, 22, and 24. In contrast, CDAS spreads both charging and discharging over a wider set of hours with smaller magnitudes, taking advantage of midday renewable surplus while avoiding the sharp swings that would require aggressive late-day cooling. In particular, the reduced BESS energy output under CDAS directly leads to a lower battery pack temperature by limiting heat generation during charge and discharge events.

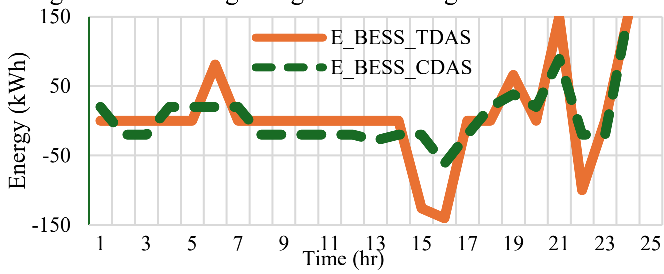

Figure 4. BESS Usage Comparison between TDAS and CDAS.

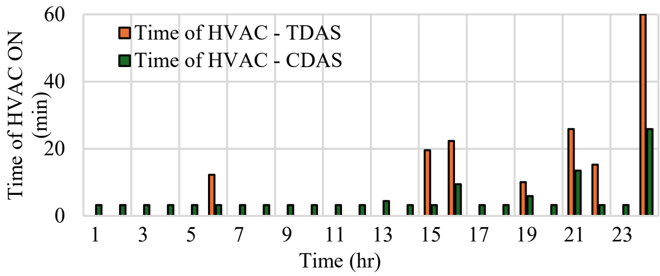

Figure 5. HVAC Runtime of TDAS and CDAS.

Figure 5 presents the corresponding HVAC operation, expressed as the number of minutes the cooling system is turned on in each hour. For TDAS, HVAC usage is highly clustered: the unit remains off for most of the horizon and then runs for long stretches during and after the large BESS events (e.g., around hours 15–16, 21–22, and especially 24), reflecting the need to "catch up" and remove a substantial amount of accumulated heat. Under CDAS, the HVAC operates more gently but more consistently, with short cooling intervals in many hours and only moderate increases during periods of heavier BESS activity. This pattern confirms that the co-optimized schedule anticipates thermal buildup and deploys cooling proactively, which both limits the maximum battery temperature and reduces total HVAC energy, in line with the aggregate values reported in Table 1.

V. Conclusion

This paper showed that treating BESS cooling as a post-compute add-on, as in a TDAS, systematically underestimates operating cost and drives more thermally aggressive battery use. The CDAS instead embeds HVAC energy directly into the optimization, so dispatch decisions are made with full knowledge of their thermal and cooling consequences. Case-study results show that CDAS keeps the battery up to 10 °C cooler, cuts HVAC energy by more than 25% and slightly lowers operating cost or keeps it at the same cost level in some circumstances, all while meeting the same reliability requirements. These findings indicate that realistic microgrid planning with BESS must co-schedule electrical and cooling loads, rather than relying on purely electrical models with post-processed thermal corrections.

VI. References

[1] J. Liu, M. S. Rahman, J. Lu and M. J. Hossain, "Performance investigation of hybrid AC/DC microgrids during mode transitions," in *Proc. 2016 Australasian Universities Power Engineering Conf. (AUPEC)*, Brisbane, QLD, Australia, 2016, pp. 1–6, doi: 10.1109/AUPEC.2016.7749320.

[2] J. C. B. Nainggolan *et al.*, "Impact of power quality of microgrids with high penetration of renewable energy on the characteristics of LED lamp," in *Proc. 2023 4th Int. Conf. High Voltage Eng. Power Syst. (ICHVEPS)*, Denpasar Bali, Indonesia, 2023, pp. 589–593, doi: 10.1109/ICHVEPS58902.2023.10257347.

[3] Black & Veatch, "Energy storage," *Black & Veatch*, Overland Park, KS, USA. Accessed Nov. 7, 2025. [Online]. Available: https://www.bv.com/en-US/what-we-do/power-delivery/energy-storage

[4] M. Hamidieh and M. Ghassemi, "Microgrids and resilience: A review," *IEEE Access*, vol. 10, pp. 106059–106080, 2022, doi: 10.1109/ACCESS.2022.3211511.

[5] H. Suyanto and R. Irawati, "Study trends and challenges of the development of microgrids," in Proc. 2017 15th Int. Conf. Quality in Research (QiR): Int. Symp. Elect. Comput. Eng., Nusa Dua, Bali, Indonesia, 2017, pp. 383–387, doi: 10.1109/QIR.2017.8168516.

[6] M. C. Kocer *et al.*, "Cloud induced PV impact on voltage profiles for real microgrids," in *Proc. 2018 5th Int. Symp. Environ.-Friendly Energies Appl. (EFEA)*, Rome, Italy, 2018, pp. 1–6, doi: 10.1109/EFEA.2018.8617080.

[7] Enel Green Power, "BESS: Battery energy storage systems," *Enel Green Power*. Accessed Nov. 7, 2025. [Online]. Available: https://www.enelgreenpower.com/learning-hub/renewable-energies/storage/bess

[8] SYSO Technologies, "Day-ahead markets: Strategic energy scheduling for battery storage and renewables," *SYSO Technologies*. Accessed Nov. 7, 2025. [Online]. Available: https://www.sysotechnologies.com/day-ahead-markets/

[9] Full Stack Energy, "Real time assets management," Full Stack Energy. Accessed Nov. 7, 2025. [Online]. Available: https://fullstackenergy.com/real-time-assets-management/

[10] M. M. Hasan, S. A. Pourmousavi, F. Bai and T. K. Saha, "The impact of temperature on battery degradation for large-scale BESS in PV plant," in *Proc. 2017 Australasian Universities Power Engineering Conf. (AUPEC)*, Melbourne, VIC, Australia, 2017, pp. 1–6.

[11] M. M. Hasan and S. A. Pourmousavi, "Battery cell temperature estimation model and cost analysis of a grid-connected PV-BESS plant," in Proc. *2019 IEEE Innovative Smart Grid Technol. – Asia* (ISGT Asia), Chengdu, China, 2019, pp. 1804–1809, doi: 10.1109/ISGT-Asia.2019.8881157.

[12] C. Liu, X. Wang, Y. Zou, H. Zhang and W. Zhang, "A probabilistic chance-constrained day-ahead scheduling model for grid-connected microgrid," in *Proc. 2017 North American Power Symp. (NAPS)*, Morgantown, WV, USA, 2017, pp. 1–6, doi: 10.1109/NAPS.2017.8107180

[13] T. Yang, X. Li, L. Qi, D. Hui and X. Jia, "A schedule method of battery energy storage system (BESS) to track day-ahead photovoltaic output power schedule based on short-term photovoltaic power prediction," in *Proc. Int. Conf. Renewable Power Gener. (RPG 2015)*, Beijing, China, 2015, pp. 1–4, doi: 10.1049/cp.2015.0316..

[14] Y. Shen, C. Liu, H. Wang, Z. Wang, Y. Song and Y. Liu, "Day-ahead scheduling for microgrid considering battery degradation rate and temperature constraints," in *Proc. 2024 Asia Conf. Adv. Electr. Power Eng. (ACEPE)*, Suzhou, China, 2024, pp. 1–6, doi: 10.1109/ACEPE63527.2024.10871689.

[15] B. Saha and K. Goebel, "Battery Data Set," NASA Prognostics Data Repository, NASA Ames Research Center, Moffett Field, CA, USA, 2007.

979-8-3315-8138-1